PROCEEDINGS OF THE ROYAL SOCIETY B

rspb.royalsocietypublishing.org

Research

Cite this article: Dorgan KM, Law CJ, Rouse GW. 2013 Meandering worms: mechanics of undulatory burrowing in muds. Proc R Soc B 280: 20122948.
http://dx.doi.org/10.1098/rspb.2012.2948

Received: 10 December 2012
Accepted: 5 February 2013

Subject Areas:
biomechanics, ecology, environmental science

Keywords:
burrowing, gait, biomechanics, kinematics, polychaete, annelida

Author for correspondence:
Kelly M. Dorgan
e-mail: kdorgan@ucsd.edu

Electronic supplementary material is available at http://dx.doi.org/10.1098/rspb.2012.2948 or via http://rspb.royalsocietypublishing.org.

Royal Society Publishing
Informing the science of the future

Meandering worms: mechanics of undulatory burrowing in muds

Kelly M. Dorgan, Chris J. Law and Greg W. Rouse

Scripps Institution of Oceanography, University of California San Diego, La Jolla, CA 92093–0202, USA

Recent work has shown that muddy sediments are elastic solids through which animals extend burrows by fracture, whereas non-cohesive granular sands fluidize around some burrowers. These different mechanical responses are reflected in the morphologies and behaviours of their respective inhabitants. However, *Armandia brevis*, a mud-burrowing opheliid polychaete, lacks an expansible anterior consistent with fracturing mud, and instead uses undulatory movements similar to those of sandfish lizards that fluidize desert sands. Here, we show that *A. brevis* neither fractures nor fluidizes sediments, but instead uses a third mechanism, plastically rearranging sediment grains to create a burrow. The curvature of the undulating body fits meander geometry used to describe rivers, and changes in curvature driven by muscle contraction are similar for swimming and burrowing worms, indicating that the same gait is used in both sediments and water. Large calculated friction forces for undulatory burrowers suggest that sediment mechanics affect undulatory and peristaltic burrowers differently; undulatory burrowing may be more effective for small worms that live in sediments not compacted or cohesive enough to extend burrows by fracture.

1. Introduction

Mechanical interactions between organisms and their environments are integral to locomotion, but mechanical responses of soils and sediments to forces applied by burrowing organisms are poorly understood. How morphologies and behaviours of infauna affect burrowing performance is important in understanding the evolution of burrowing animals and the ecology of sediment communities. Many worms with diverse morphologies and behaviours extend burrows through muddy sediments by fracture, using eversible mouth parts and muscular expansions to apply dorsoventral forces to burrow walls that are amplified at the burrow tip [1–3]. Fracture of muddy sediments results not only from direct forces applied by burrowers, but also from hydraulic pumping by infauna during burrow irrigation [4].

Nematodes and some polychaetes, however, lack expansible anteriors used for burrow extension by fracture, and instead move through muddy sediments by undulation [5]. For these organisms, kinematics are similar to those of sandfish lizards, which use body undulations rather than limbs to generate thrust and fluidize desert sands [6]. Fluidization of the medium is indicated by backward slipping of the animal and bulk transport of suspended grains in the opposite direction of locomotion. Mechanical responses differ, however, among burrowers in non-cohesive granular sands: fishes such as sand lances and eels burrow in saturated marine sands with no slipping [7,8]. Kinematics are similar to terrestrial crawling, and burrowing results in small discrete movements of sand grains rather than bulk transport. In both cases, movement involves displacement of discrete grains against gravitational forces, in contrast to elastic muds, which are held together by adhesion and cohesion of the intra-granular organic matrix [9].

These different responses of sands to undulatory burrowers are quantified using wave efficiency, $\eta = v_x/v_w$, the ratio of the animal's forward velocity, v_x, to the velocity of the posteriorly travelling undulatory wave, v_w. Wave efficiencies of $\eta \approx 0.5$ for burrowing sandfish lizards are consistent with fluidization of granular sand [6], and of $\eta \approx 1$ for sand lances and eels are consistent with a solid response of sand [7,8]. For swimming animals, wave efficiency varies

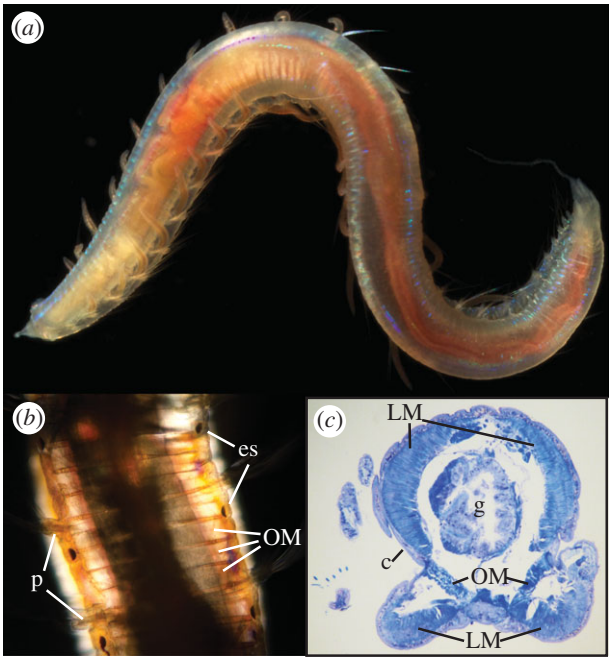

Figure 1. (*a*) Morphology of *Armandia brevis*. (*b*) Ventral view of oblique muscles (OM) shown using polarized light microscopy with segments distinguished by parapodia (p) and segmental eye spots (es). (*c*) Cross-section of internal anatomy showing large bands of oblique (OM) and longitudinal muscle (LM), gut (g), and cuticle (c). (Online version in colour.)

considerably and depends on Reynolds number (*Re*) [10], with high values of greater than 0.7 for swimming eels [11,12] down to 0.23 for sperm [13]. For swimming leeches, η is proportional to size and drops from 0.55 to 0.43 with a 10-fold increase in viscosity [14]. Crawling animals have high η, greater than 0.8 compared with 0.19–0.29 for swimming nematodes [5], approaching 1 on surfaces with sufficient friction in which no slipping occurs.

Undulatory burrowing has not yet been quantitatively explored in muddy sediments, which are elastic solids that differ mechanically from non-cohesive sands [9]. *Armandia brevis* (Moore, 1906), an opheliid polychaete that inhabits muddy to sandy sediments, lacks both eversible mouthparts and circular muscles needed for peristalsis. Rather, it has bands of oblique muscles that act antagonistically to longitudinal muscles, enabling lateral bending and undulatory movements (figure 1). *Armandia brevis* also swims by undulation, enabling direct comparison of wave efficiency while burrowing and swimming. Wave efficiency values for burrowing *A. brevis* close to 1 and higher than that of swimming worms would indicate solid response of the medium, whereas $\eta \ll 1$ would indicate fluidization.

For *A. brevis*, swimming is a derived behaviour—apart from this taxon and other members of its own subfamily Opheliniae, no other opheliid swims [15]. Though dispersal is one explanation, most swimming *A. brevis* are reproductive, and spawning occurs only once before death [16]. That swimming seems to be a secondary mode of locomotion raises the question of whether swimming behaviours are distinct from burrowing, i.e. whether the same gait is used in both media with kinematic differences attributable to mechanics of solids compared with fluids.

Discrete gaits are characterized by discontinuous changes in movement patterns. Both sandfish lizards and sandlance fishes substantially change their body shapes, increasing the amplitude relative to wavelength (A/λ), when transitioning to burrowing from running and swimming, respectively [6,7]. Larger A, λ and frequency have been observed for nematode worms swimming in water compared with media with higher resistance, but positive linear relationships indicate constant A/λ and reveal no discrete transition indicative of gait change [17,18]. Although the transition from fluid to elastic mud is inherently discontinuous, similar body shape of *A. brevis*, characterized by A/λ, would be consistent with the same gait used in both media. As body shape is determined from discrete time points and is affected by external forces [19], we also compared changes in body angle over a cycle of undulatory movement as well as patterns of body curvature to determine whether burrowing and swimming gaits are the same. Whereas undulatory movements have been described as sinusoidal [10] and a best-fit sine function has been used for measuring amplitude, wavelength and wave speed [6], curvature of the path of *A. brevis* appeared flatter and broader than a sine function. Similar geometry was first described for paths of meandering rivers, which can be approximated as a sine-generated curve; the relationship between direction angle of the path, θ, and distance along the path, s, fits a sine curve [20]. A sine fit to θ–s is a better approximation of snake shape than an x–y sine fit, consistent with waves of alternating muscle contraction travelling along the length of the animal changing the body curvature [21]. Direct measurement of kinematic parameters such as amplitude, wavelength, radius of curvature and v_w from profiles enables comparisons, but lacks a mechanistic basis; fit to a meander curve would be consistent with sinusoidal muscle contraction and relaxation, whereas deviations indicate non-sinusoidal contraction or non-uniform external forces.

We explored the burrowing and swimming behaviour of *A. brevis* and combined experiments with theory to assess three hypotheses for the mechanism of undulatory burrow extension in muds: (i) *A. brevis* extends burrows by fracture [1], (ii) *A. brevis* fluidizes muddy sediments, indicated by $\eta \ll 1$[6], and (iii) the muddy sediment deforms plastically through grain rearrangement, indicated by $\eta \approx 1$ [7,8].

2. Material and methods

To address whether *A. brevis* extends burrows by fracture, we combined experiments on worms in gelatin, an analogue for cohesive elastic muds through which worms burrow by fracture [1–3], with theoretical predictions based on linear elastic fracture mechanics (LEFM). Because *A. brevis* lives in surface sediments [16], we developed an additional analogue for weak surface muds comprising organic-mineral aggregates, fragments of concentrated gelatin, in which kinematics were analysed to determine whether fluidization or solid grain rearrangement occurs. Kinematics of burrowing and swimming worms were compared to assess whether *A. brevis* uses the same gait in the different media.

(a) Kinematics

Armandia brevis were collected from shallow subtidal sediments in Mission Bay, San Diego, CA, and from sediments in the flowing seawater tanks at Scripps Institution of Oceanography, La Jolla, CA. For experiments to determine whether worms burrowed by fracture, glass aquaria were filled with seawater gelatin (28.35 g l^{-1}), and worms were placed in pre-made cracks and filmed following methods of Che & Dorgan [3]. For elastic aggregate burrowing experiments, concentrated seawater gelatin (85 g l^{-1}) was chopped in a food processor to fragments

roughly 200–500 µm diameter. Gelatin pieces were slowly added to a plexiglass ant farm aquarium (7 × 7 × 1.5 cm) with seawater and were gently mixed to remove air bubbles. Worms were placed below the surface of the aggregates equidistant from the two walls of the aquarium, and movements were recorded. Only video segments in which the worms moved in a plane perpendicular to the camera angle (in focus within an approx. 1 cm focal plane) and did not reach either wall were used for analysis. Worms were filmed swimming in a Petri dish (10 × 2 cm) with a Canon T2i DSLR camera at 60 fps. For both burrowing and swimming, wall effects may occur, but eliminating or substantially reducing wall effects was logistically difficult because of visualization of burrowing worms and the speed of swimming worms. Videos were first subsampled using QuickTime Pro v. 7 (swimming) or LabView v. 7.1 (burrowing), and processed in ImageJ v. 1.44 to obtain body outlines and head and tail positions for each frame.

To characterize gait, first body shape was analysed by measuring amplitude and wavelength. From outline coordinates and head and tail positions, midlines were calculated and further analysis done using custom Matlab (R2010B) scripts. To measure amplitude and wavelength, curvature of the path of travel (smoothed centre of mass (COM) path) was removed by sequentially rotating the midline for each frame and later frames about the COM for that frame. Next, maximum deviations of midlines from that straightened path and distances between peaks were calculated. For consistency, midlines were shortened to total body length, L_s, of 95 per cent of the shortest midline in a sequence.

We compared fits with a meander curve and sine curve for both burrowing and swimming worms. Shortened midlines were converted from x–y to θ–s coordinates using a cartesian-to-polar coordinate conversion for each segment ds of the midline. Best-fit sine function in x–y coordinates was the sine fit, in θ–s coordinates was the meander fit. Because both sine and meander curves were fit to a line of points, residuals were not randomly distributed and the autocorrelation of midline points likely resulted in inflated R^2, but subsampling did not effectively remove the autocorrelation or change the R^2. To better assess the fit of the two models, we also compared the body angle, sin(θ), and curvature, dθ/ds, profiles to those predicted by a sine and meander fit (see the electronic supplementary materials for details). The sine and meander curves were fit to individual frames rather than the path, for which both amplitude and wavelength varied considerably, making modelling the path as a single travelling sine wave infeasible.

Wave efficiency was calculated as $\eta = v_x/v_w$, where the wave velocity in θ–s coordinates calculated from cross correlation of subsequent frames was transformed to x–y coordinates by the sinuosity, the ratio of the body length (before shortening) to the shortest distance from head to tail, to obtain v_w. Sinuosity was inflated for swimming worms by yaw, seen as side-to-side movement of the COM, so rather than using v_x calculated from the smoothed COM path, velocity was calculated along the unsmoothed COM path (greater than v_x for swimming, but approx. v_x for burrowing) and this corrected velocity was used in wave efficiency calculations.

(b) Model

LEFM theory was used to calculate a force balance for burrow extension by fracture for an undulating worm. Forces resisting forward movement in linear elastic muds include cohesive fracture resistance, elastic resistance to sediment deformation and friction. The work to extend a burrow by fracture is the sum of the work of fracture, $W_{Cr} = G_c(\Delta x)w_{cr}$, and the elastic work, $W_{El} = 2\sigma_w\ w_w(\Delta x)h$ [22]. G_c is the fracture toughness (J m^{-2}), Δx is the distance the crack extends (m), w_{cr} is the crack width (m), σ_w is the internal pressure of the worm (Pa), w_w is the width of the worm (m) and h is the half-thickness measured dorsoventrally (m). A factor of 2 is included because elastic displacement occurs along both dorsal and ventral crack surfaces. Thrust force, $F_{Cr} + F_{El}$, required to drive a wedge-shaped worm forward a distance Δx must balance the resistance:

$$(F_{Cr} + F_{El})\Delta x - [G_c(\Delta x)w_{cr} + 2\sigma_w w_w(\Delta x)h] = 0. \tag{2.1}$$

For peristaltic burrowing, friction is ignored because the normal force on narrow moving segments is greatly reduced by nearby dilated stationary segments, an assumption that does not apply to more rigid-bodied undulatory burrowers. Here, we include a friction force, $F_{Fr} = 2\ \mu\sigma_w w_w L$, with normal force based on elasticity, which acts along L, the entire length of the worm (m). In a crack-shaped burrow, friction acts on both dorsal and ventral surfaces (requiring a factor of 2). In sediments with density greater than that of the worm, overlying weight also contributes to friction and F_{El}, but in gelatin, this term is small and can be ignored.

Rather than travelling in a straight line, undulatory movement occurs in a two-dimensional plane. Resistive forces occur along the body axis, s, and we calculate total external resistive forces as

$$\begin{aligned} F_{res}(s) &= F_{Cr}(s) + F_{El}(s) + F_{Fr}(s) \\ &= G_c w_{cr} + 2\sigma_w w_w h + \int_0^L 2\mu\sigma_w w_w \mathrm{d}s. \end{aligned} \tag{2.2}$$

During undulation, thrust, F_{Th}, is applied normal (n) to the body axis, and here, we assume that these normal forces, $F_{Th}(n)$, are limited by material resistance rather than the amount of muscular force the worm can generate. Assuming that burrow extension follows LEFM and the burrow is a planar crack compressing the worm dorsoventrally [1], material resistance to these lateral forces is limited by the lateral fracture resistance. Maximum lateral thrust force, therefore, depends on the lateral work of fracture, elastic work and friction, the same components as axial resistance but differing in geometry. For lateral resistance, the crack length is the axial length of the worm, L, rather than w_{cr}:

$$\begin{aligned} F_{Th}(n) &= F_{Cr}(n) + F_{El}(n) + F_{Fr}(n) \\ &= \int_0^L G_c \mathrm{d}s + \int_0^L 2\sigma_w h \mathrm{d}s + \int_0^L 2\mu\sigma_w w_w \mathrm{d}s. \end{aligned} \tag{2.3}$$

In reality, thrust force is not applied along the entire length of the worm or at the maximum possible magnitude, so a scaling factor $T(s) \in [0, 1]$ is incorporated into equation (2.3). This thrust force, $F_{Th}(n)T(s)$, results in an added (to F_{res}) frictional resistance term proportional to the thrust and distributed along L on the outer curved side of the body, $F_{Fr\_added}(s) = \mu F_{Th}T(s)$.

Axial resistive forces and lateral thrust forces are balanced by the curvature of the body (figure 2*a*). Converting to x–y coordinates with the x-axis aligned with the s-axis at $L = 0$ (when the head is oriented parallel to velocity, with $\theta\sigma$ the body angle), and assuming steady state,

$$F_{res}(s)cos\theta + F_{Th}(n)T(s)sin\theta = 0. \tag{2.4}$$

The internal pressure of the worm, σ_w, depends on the material stiffness, E, and the elastic displacement, here h, the half-thickness of the worm, as well as the crack geometry. For the peristaltic burrowing polychaete *Cirriformia moorei* (Blake, 1996), this value was determined from measured displacements along the length of the body and material stiffness using a two-dimensional finite-element model [22]. Elastic modulus, E, relates stress to strain in a material, but for burrowers, relating displacement (h) to strain ($\varepsilon = h$/length scale) is confounded by what length scale to use. We can calculate from *C. moorei*

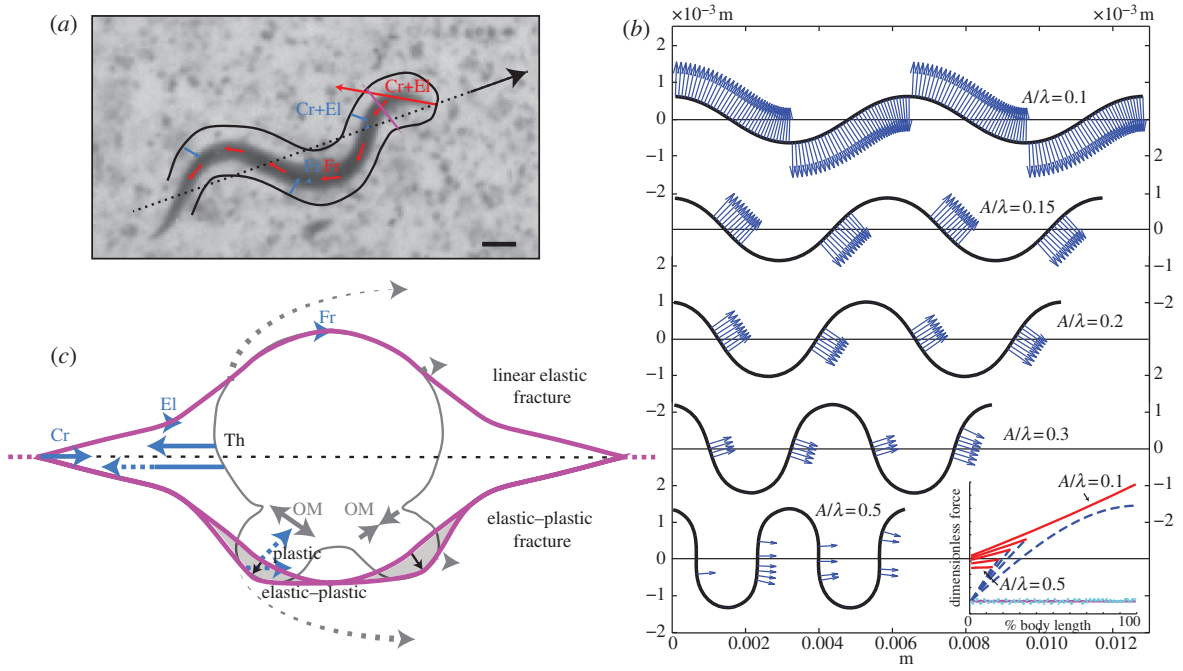

Figure 2. (*a*) Schematic dorsal view of forces resisting movement (solid line) and forces generating thrust (arrows) against lateral crack edges, calculated from linear elastic fracture mechanics (LEFM), with lengths proportional to calculated magnitudes. Thrust forces applied normal to the curved body must balance axial resistance from friction (Fr) and anterior fracture (Cr) and elastic (El) resistance to burrow (scale bar, 2 mm). (*b*) Modelled *Armandia brevis* with ideal meander shapes ($A/\lambda = 0.1$ to 0.5; black lines) with distribution of normal forces (arrows) necessary based on LEFM to overcome resistive forces along the body. (inset) Relative thrust (upper dashed lines) and resistance (upper solid lines) in the *x*-direction and in the *y*-direction (lower dashed and solid lines, respectively) are plotted as a function of increasing % body length over which $T(s) = 1$ is applied. Modelled results for y-direction forces are shown only for $A/\lambda = 0.1$ but are representative of all values of A/λ. (*c*) Schematic cross-section view of forces generating thrust against lateral crack edges. Maximum thrust (Th) is limited primarily by fracture resistance under LEFM, but plastic deformation, here illustrated on the ventral side, could increase lateral resistance through work to plastically deform sediment with additional elastic–plastic resistance resulting from the deformed geometry (hypothetical forces shown as dotted lines; oblique muscles (OM) shown connecting lateral and ventral grooves). (Online version in colour.)

results a scale factor as a function of the geometry, $f(g)$ (m^{-1}),

$$\sigma_w = E\varepsilon \approx Ehf(g). \tag{2.5}$$

Finite-element modelling shows that $f(g)$ depends primarily on the distance from the worm to the lateral crack edge and that only a twofold increase in body thickness occurred as the crack tip was extended from the lateral side of the worm out to a large distance at which thickness reached an asymptote, with σ_w and E held constant. These results suggest that differences in $f(g)$ between *C. moorei* and *A. brevis* do not exceed a factor of 2 and are probably much smaller (cf. fig. 7*b* in [2]).

Applying the assumption in equation (2.5), assuming that the crack width is related to worm width as $w_{cr} = aw_w$, and rearranging to obtain non-dimensional terms, the force balance (equation (2.4)) becomes

$$\frac{\int_0^L T(s)\sin(\theta)\mathrm{d}s}{w_w} = \frac{aG_c/Eh^2f(g) + 2 + 2\mu\int_0^L \cos(\theta)\mathrm{d}s/h + \mu\psi\int_0^L T(s)\cos\theta\mathrm{d}s/w_w}{G_c/Eh^2f(g) + 2 + 2\mu w_w/h,} \tag{2.6}$$

where

$$\psi = \frac{G_c}{Eh^2f(g)} + 2 + \frac{2\mu w_w}{h}. \tag{2.7}$$

The right-hand side of equation (2.6) is the ratio of non-dimensional resistive forces to non-dimensional maximum thrust forces, ψ, and the left-hand side indicates over what length of the body those thrust forces must be applied for forces to balance.

To compare the relative importance of fracture resistance, elasticity and friction for *A. brevis*, we use values for worm geometry and material properties to calculate approximate values for the non-dimensional terms in equation (2.6). Measured for *A. brevis*, $L = 14$ mm, $w_w = 0.7$ mm, $h = 0.35$ mm; for gelatin, $E = 7100$ Pa [3], $G_c = 0.4$ J m^{-2} [3,23], calculated from *C. moorei*, $f_1(g) = 50$ m^{-1} [22] and $a = 2$ [3], and we assume $\mu = 0.3$. For sinuosity of approximately 1.3, $\int\cos(\theta)\mathrm{d}s \approx 0.75L$. Next, the length along the body over which thrust must be applied for forces to balance and the corresponding added friction were calculated numerically for simulated worms with ratios of amplitude to wavelength, A/λ, varying from 0.1 to 0.5. Worms were modelled as cosine-derived ideal meander curves using custom MATLAB scripts. For a meander curve derived from a cosine curve, for which the head of the worm was oriented at θ, the balance of resistance, $F_{res}(s)$, and thrust, $F_{Th}(n)$, was calculated by converting from s–n to x–y coordinates, with the x-axis oriented along the COM path. This force balance in the x-direction is

$$\frac{\int_0^L T(s)\sin(\theta)\mathrm{d}s}{w_w} = \frac{a(G_c/Eh^2f(g))\cos\theta_0 + 2\cos\theta_0 + 2\mu\int_0^L \cos(\theta)\mathrm{d}s/h + \mu\psi\int_0^L T(s)\cos\theta\mathrm{d}s/w_w}{G_c/Eh^2f(g) + 2 + 2\mu w_w/h} \tag{2.8}$$

and in the y-direction, perpendicular to the COM path,

$$\frac{\int_0^L T(s)\cos(\theta)\mathrm{d}s}{w_w} = \frac{a(G_c/Eh^2f(g))\sin\theta_0 + 2\sin\theta_0 + 2\mu\int_0^L \sin(\theta)\mathrm{d}s/h + \mu\psi\int_0^L T(s)\sin\theta\mathrm{d}s/w_w}{G_c/Eh^2f(g) + 2 + 2\mu w_w/h}. \tag{2.9}$$

Maximum possible thrust was applied ($T(s) = 1$) along an increasing percentage of the body until thrust forces and resistive forces balanced (left side of equation (2.8) exceeded the right side). We chose this approach rather than using a constant $T(s)$ along the length of the worm both to minimize the added friction term, $F_{Fr\_added}(s)$, and to be consistent with qualitative observations of focused forces applied by the related *Ophelina acuminata* (Orsted, 1843) moving in a pre-made crack in gelatin visualized using photoelastic stress analysis (K. M. Dorgan 2009, unpublished data). Force was applied in the direction normal to the modelled midline and opposite the direction of forward movement. The force balance in the y-direction was used to determine at what position ds to increase $T(s)$. $T(s)$ was incrementally increased at the position at which θ was closest to the ratio of the discrepancy in the y-direction force balance (difference between right and left sides of equation (2.9)) relative to the discrepancy in the x-direction force balance (difference between right and left sides of equation (2.8)) until the x-direction thrust force exceeded resistance.

3. Results and discussion

(a) *Armandia brevis* does not extend burrows by linear elastic fracture

Worms placed in different orientations in pre-formed cracks of varying widths in gelatin, an analogue for elastic muds, exhibited undulatory movements with small-amplitude head wiggling, but no worms extended the burrow even when curved with the posterior braced against the crack edge ($n > 10$). Shapes of crawling snakes depend primarily on external forces, specifically the ratio of lateral resistance to gravitational force (which determines the normal force upon which ventral friction depends): if lateral resistance is low relative to friction, the body is more curved [19]. *Armandia brevis*, oriented dorsoventrally compressed in a crack, experienced low lateral resistance compared with dorsoventral friction augmented by fracture resistance.

Modelling results showed that relative magnitudes of dimensionless components of axial resistance (right side numerator, equation (2.6)) are: fracture component, $aG_c/Eh^2 f_1(g) = 18$; elastic work associated with burrow extension, 2; friction component, 18; and added friction depends on $T(s)$, and is calculated numerically. Fracture resistance higher than elastic resistance is consistent with calculations for *C. moorei* of a work of fracture approximately 10× elastic work [22]. Relative magnitudes of dimensionless components of lateral thrust (right side denominator, equation (2.6)) are: fracture component, 9; elastic work, 2; and friction, 1 (figure 2*a*). That friction plays a substantial role in resisting axial movement but does little to preventing lateral slipping is consistent with the elongate shape of the worm.

For small A/λ, maximum thrust forces along the entire length of the worm were insufficient to balance resistive forces; as A/λ increased, thrust forces applied along decreasing percentages of the body could balance resistance (figure 2*b*). The relative thrust force (left side of equation (2.8), dashed lines in figure 2*b* inset) increased as $T(s)$ increased, reaching the resistive forces relative to maximum thrust (right side of equation (2.8); solid lines) for $A/\lambda > 0.1$. Added friction from thrust forces increased the resistance forces (solid lines in figure 2*b* inset) substantially, to approximately 2.5× the resistance force with no added friction for $A/\lambda = 0.1$. As A/λ increased, initial resistance force decreased owing to a decrease in the x-component of friction, and the added friction from thrust increased less steeply because as θ increases, more of the added friction acts in the y-direction. $T(s)$ was increased at positions along the length of the worm to maintain equilibrium in the y-direction—the resistance (right side of equation (2.9), solid line in figure 2*b* inset) was close to zero and thrust (left side of equation (2.9), dashed line in figure 2*b* inset) fluctuated around 0. $T(s)$ was more variable for the largest A/λ, 0.5, owing to the many positions at which $\theta \approx \pi/2$, and indicates that forces smaller than maximal forces could be distributed along this region of the body. Even at intermediate A/λ, the substantial portion of the body required to exert the maximum possible force indicates that the LEFM model is only barely mechanically feasible. Our model applies maximum forces; exceeding these would result in lateral crack extension and reduced lateral resistance. Applying smaller forces by reducing $T(s)$, however, would require force to be applied along a greater percentage of the body, increasing the added friction, which is already substantial at low-to-intermediate A/λ (figure 2*b*). Only at very high A/λ does this mechanism seems mechanically feasible, but at high A/λ efficiency is low and manoeuverability may be limited.

(b) Non-cohesive granular media exhibits solid response to undulatory burrowing

Based on LEFM, lateral fracture resistance is only barely sufficient for *A. brevis* to overcome anterior resistance, but dorsoventral plastic deformation of sediments could increase resistance to lateral slipping (figure 2*c*). In natural muds, fracture toughness and stiffness are low in the top approximately 2–3 cm of sediments [24,25], corresponding to the depth distribution of *A. brevis* [16]. At the surface, fracture toughness approaches zero, indicating that surface muds are non-cohesive, high-porosity aggregates and that linear elastic fracture occurs only below the surface layer. *Armandia brevis* was able to burrow through an analogue of non-cohesive elastic fragments of gelatin simulating surficial, unconsolidated sediments comprising organic-mineral aggregates (see the electronic supplementary materials, movie S1). Elastic–plastic fracture with dorsoventral plastic deformation is, however, theoretically feasible and, assuming a gradient in sediments from surface aggregates to cohesive elastic mud, would increase worms' depth limit. Ventral and lateral grooves increase the angle of contact between the worm and sediment, probably increasing lateral resistance and facilitating elastic–plastic fracture (figure 2*c*).

Worms burrowed through this analogue material with a non-slipping undulatory wave (figure 3*a*), consistent with the hypothesis of sediment exhibiting solid behaviour with plastic reorganization of grains. By contrast, worms swimming through a fluid medium clearly slip backwards (see the electronic supplementary material, movie S2; figure 3*b*). Wave efficiencies were significantly higher for burrowing than for swimming worms (figure 4*a*). For burrowing worms, $\eta = 1.00 \pm 0.10$ (mean ± s.d.), and for swimming worms, $\eta = 0.58 \pm 0.11$, similar to values of 0.50–0.58 for the related *Ophelina* sp. [26] and of approximately 0.5 for burrowing sandfish lizards that fluidize sands [6]. Calculating wave efficiency from smoothed v_x values rather than from velocity along the unsmoothed COM path results in $\eta = 0.48 \pm 0.10$ for swimming worms and $\eta = 0.97 \pm 0.11$ for burrowing worms. Faster swimming worms slipped less, consistent with dependence on *Re*, whereas no relationship was observed between η and velocity for

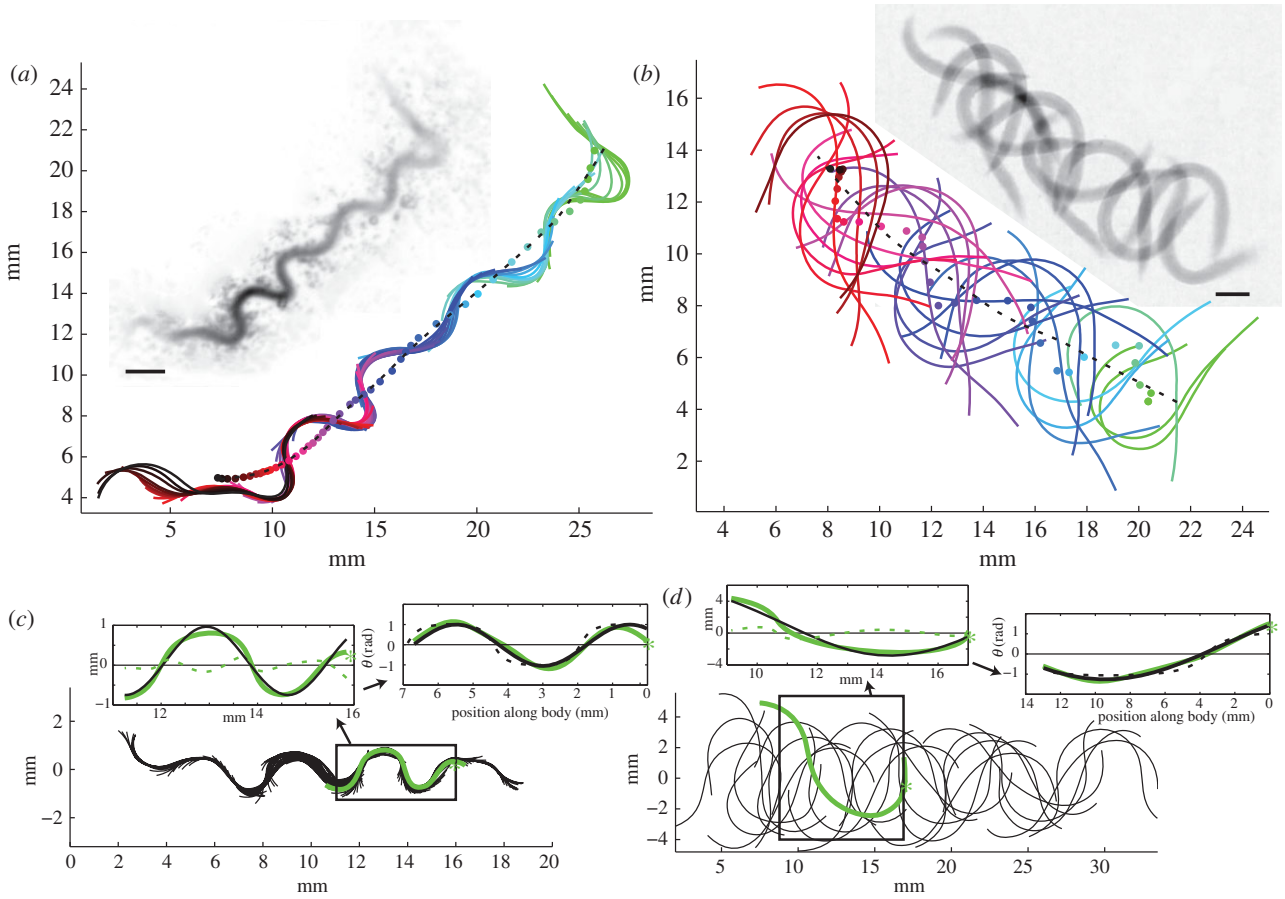

Figure 3. Midlines of *A. brevis* (*a*) burrowing (at 0.067 s intervals) and (*b*) swimming (at 0.017 s intervals), coloured sequentially from green to black with corresponding centre of mass as solid circles (dotted black line is smoothed COM path). Raw images superimposed are shown in insets (scale bar, 2 mm). For both (*c*) burrowing and (*d*) swimming, a sine fit (solid black) through midlines (solid line with asterisk (*) at head) does not match curvature (residuals in dotted line) as well as a meander fit to body angle, θ, as a function of body position, s (black dotted line shows the converted sine fit). (Online version in colour.)

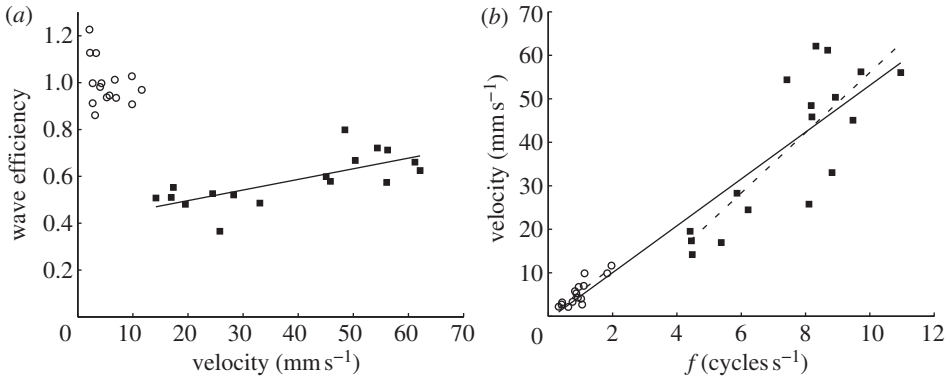

Figure 4. Parameters quantifying gait for burrowing (open circles) and swimming (fillled squares). (*a*) Wave efficiency is correlated with velocity for swimming ($R^2 = 0.52$; $p < 0.01$), but not for burrowing worms. (*b*) Distances travelled per cycle for burrowing (5.7 $\pm$ 2.0 mm cycle^{-1}, mean $\pm$ 95% CI; $R^2 = 0.74$) and swimming (6.9 $\pm$ 2.6 mm cycle^{-1}; $R^2 = 0.67$) do not differ (combined data, solid line; 5.4 $\pm$ 0.8 mm cycle^{-1}, $R^2 = 0.87$).

burrowing worms (figure 4*a*). Velocity showed a strong dependence on cycle frequency for both burrowing and swimming (figure 4*b*). Swimming worms travelled the same distance per cycle as burrowing worms (figure 4*b*), suggesting that inertia may balance backward slipping.

(c) Undulatory kinematics fit a meander curve

Meander curves showed good fit, significantly better than x–y sine curve fits for both burrowing (12/15 worms) and swimming (17/17 worms) when comparing frames for individual worms (see figure 3*c*,*d* and electronic supplementary material, table S1). R^2 was high, however, and more variable across individuals for both meander (0.94 $\pm$ 0.03 for burrowing; 0.99 $\pm$ 0.01 for swimming; mean $\pm$ s.d.) and sine (0.91 $\pm$ 0.03 for burrowing; 0.95 $\pm$ 0.03 for swimming) fits, probably inflated by autocorrelation of midline points (see figure 3*c*,*d* and electronic supplementary material, table S1). More substantial differences between sine and meander fits were found for body angle profiles, with R^2 for meander fits

of 0.84 ± 0.06 and 0.96 ± 0.02, and for sine fits of 0.45 ± 0.08 and 0.47 ± 0.07 for burrowing and swimming, respectively (see the electronic supplementary material, figure S1 and table S1). For swimming worms, curvature profiles also fit a meander curve significantly better than a sine curve (see the electronic supplementary material, table S1). Midline profiles, as well as body angle and curvature, of swimming worms showed a better fit than burrowing worms (see the electronic supplementary material, table S1). However, worms burrowed with smaller λ/L than when swimming, and we re-analysed the meander fit of each half of the body length of burrowing worms (because $\lambda/L \sim 0.5$); this increased the fit for burrowing worms, removing differences in fits of body shape and curvature between burrowing and swimming worms and substantially reducing the difference for body angle (see the electronic supplementary material, table S1).

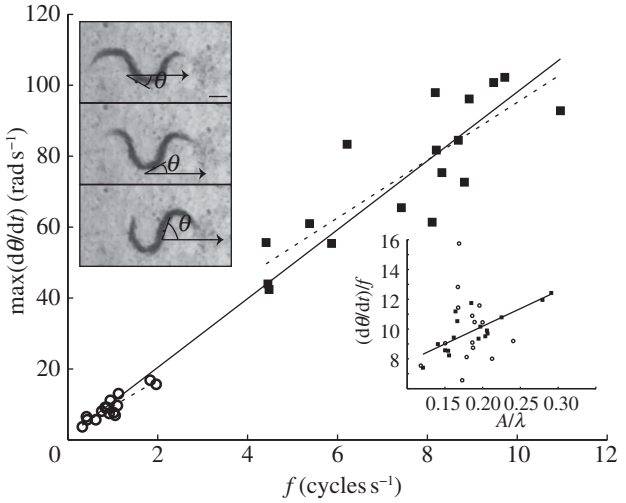

Figure 5. The amplitude of the sinusoidal relationship of $d\theta/dt$ as a function of time is strongly correlated with cycle frequency ($R^2 = 0.95$) with slopes not significantly different for burrowing (open circles), swimming (closed squares), and combined data (at 95% CI). For swimming worms (inset), some variability can be explained by a positive correlation ($R^2 = 0.61$, $p < 0.05$) between slopes calculated for individual worms [$\max(d\theta/dt)/f$ (rad s^{-1})/(cycles s^{-1})] and A/λ—faster muscle contraction per cycle results in larger A/λ. Sequential images of a burrowing worm (0.067 s apart) show changing θ (upper inset; scale bar, 2 mm).

(d) The same gait is used for burrowing and swimming

Swimming worms undulated with significantly larger amplitudes and wavelengths and at higher cycle frequencies (f) than burrowing worms (all ANOVA $p < 0.001$; electronic supplementary material, table S2 and figure S2). Higher f for swimming worms corresponds with higher velocities, and there are no obvious discontinuities for burrowing and swimming, with similar distances travelled per cycle in both media (figure 4*b*). Moreover, body shapes, quantified by A/λ, were the same, 0.18 ± 0.03 (mean ± s.d.) for burrowing and 0.19 ± 0.05 for swimming worms, similar to nematodes [5,17] and burrowing sandfish [6]. Similar body shapes (A/λ) are consistent with the hypothesis that burrowing and swimming worms use the same gait [17,18], but body shape depends primarily on external forces [19]. For undulating fishes, increasing amplitude from head to tail corresponds with lags between waves of body curvature and muscle activity [27], but constant amplitude along the length of *A. brevis* enables use of change in curvature as a first-order approximation of muscle activity. The relationship between muscle activation and body curvature is complex [28], and changes in curvature are also influenced by internal elasticity and external forces [19]; however, similar changes in curvature in the two media are consistent with similar muscle activity patterns. As a meander curve, the relationship between θ at a fixed location on the worm and time is sinusoidal, as is the relationship between $d\theta/dt$ and time. Amplitude, maximum $d\theta/dt$ per cycle (see the electronic supplementary material, figure S3), shows a strong linear relationship with f with no discontinuities that would indicate a gait transition (figure 5). Linearity indicates that the rate of body bending, presumably resulting from the rate of muscle contraction, used in both modes of locomotion is directly proportional to the cycle frequency, which is in turn directly proportional to velocity (figure 4*b*): the pattern of movement does not change with speed. More importantly, this pattern of movement does not differ between burrowing and swimming. Similar fit to a meander curve of body shape, body angle and curvature (see the electronic supplementary material, figure S1 and table S1) indicates that muscle contraction is similar and probably sinusoidal along the length of the body for both swimming and burrowing worms. Larger A and λ for swimming worms can be attributed to low resistance of water to internal elastic forces. For the nematode *C. elegans*, crawling worms experience comparable external loads and internal elastic forces, whereas for swimming worms external forces are much smaller than internal elasticity [18].

4. Conclusions

Whereas transitions from swimming to burrowing [7,8] and from running to burrowing [6] involve substantial changes in locomotory behaviour, undulatory burrowing worms change only the frequency of movement when transitioning to swimming, a derived mode of locomotion in this group [15]. Use of a burrowing undulatory gait for swimming could explain why neither *A. brevis*, most nematodes [5], nor larval lampreys [29] swim with undulatory waves increasing in amplitude, in contrast to most elongate undulatory swimmers, e.g. snakes [30], eels [11] and amphioxus [31]. Muscle contraction patterns and body stiffness contribute to this increasing amplitude [30,31], which reduces yaw, probably resulting in greater efficiency [5]. This side-to-side movement of swimming *A. brevis* (figure 3*b*) may reduce swimming efficiency but does not affect burrowing, their primary mode of locomotion.

Fit to a meander curve explicitly links the shapes of elongate animals to the muscular activity that drives movement. This sinusoidal change in angle along a path or over time describes shapes of rivers [20], snakes [21], flagella [32], *A. brevis* and probably other biological and abiotic elongate patterns as well. In animal locomotion, deviations from this meander model shape may indicate non-uniform external forces or alterations of behaviour. For *A. brevis*, similarity in meander fit supports our hypothesis that swimming worms use the same muscle contraction patterns but at higher frequency than burrowing worms.

Our finding that LEFM is an unlikely mechanism for undulatory burrowing in muds is based on the size of *A. brevis* and limited data for mechanical properties of muds. Behaviours of burrowers using fracture depend on

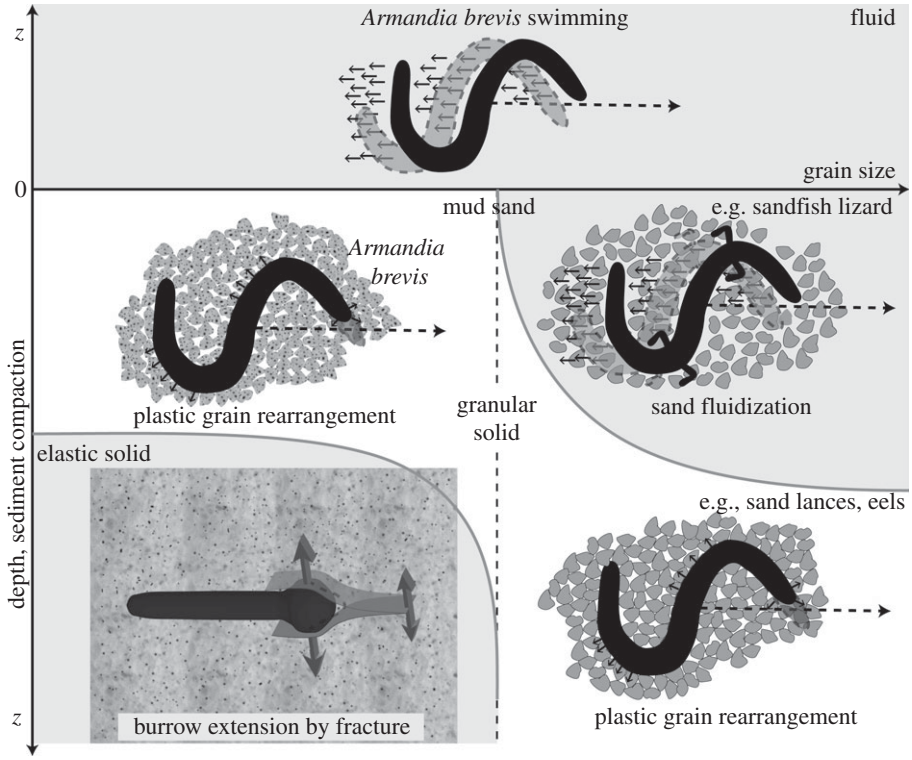

Figure 6. Scheme of different mechanisms of burrowing in idealized muds (left) and sands (right). Dotted line indicates a later time, and the differing mechanics of the media are indicated. Plastic grain rearrangement by *Armandia brevis* (upper left) is consistent with descriptions of kinematics of non-slipping burrowing in sands [7,8] (lower right), although in muds, aggregate grains have lower density and are deformable, suggesting that friction may be more important and gravity less important than in sands. This solid granular response differs from sand fluidization (upper right), which has thus far only been observed in dry terrestrial sands by lizards considerably larger than *A. brevis* [6]. Depth or sediment compaction is hypothesized to distinguish between the two mechanisms in each sediment type, but more research is needed on the mechanical responses of natural sediments to burrowing behaviours on spatial scales corresponding to burrower morphologies. Many natural sediments are heterogeneous mixtures of sand and mud and probably exhibit properties of both media. Lower left panel of burrow extension by fracture adapted from Dorgan *et al*. [1] with permission.

the ratio of work of fracture ($\propto G_c$, fracture toughness) to elastic work ($\propto Eh$, stiffness and body thickness) [23]. For peristaltic burrowing, work of fracture is approximately 10× elastic work [22], but for undulatory burrowers, this large friction component that in elastic gels depends primarily on stiffness, E, combines with elastic work, altering this ratio. Compared with its behaviour with peristaltic burrowers, the same material would seem much stiffer. For smaller undulatory burrowers like the nematode *C. elegans*, G_c/Eh is much higher than for *A. brevis*, possibly explaining their ability to burrow through gelatin [17] and agar. Similarly, in soft sediments with higher G_c/E than gelatin, friction would be less important and fracture a more feasible mechanism of undulatory burrowing. Friction increases not only the apparent stiffness of muds, but also total work to burrow, potentially exceeding the muscle capacity of *A. brevis* in deeper sediments (a possible explanation for the large longitudinal muscle bands, figure 1*c*). Friction is probably high regardless of sediment mechanics: in weak sediments with less elastic cohesion, the normal force depends primarily on overlying weight, and friction would increase with depth, similar to in elastic muds with increasing E. Sediments with heterogeneous mixtures of sand and mud are common habitats for burrowers and probably have mechanics that fall between those of sands and muds. The similar granular responses of surface muds on small scales and of sands to larger burrowers (figure 6) and the potential use of elastic–plastic fracture suggest interesting hypotheses about burrowing in heterogeneous sandy muds, which may involve a combination of elastic and granular mechanisms that depend on burrower size, morphology and behaviour, as well as small-scale differences in sediment mechanics.

Muddy sediments are ubiquitous and are inhabited by diverse animals, many of which, such as *A. brevis*, are small, live close to the sediment–water interface, and exhibit undulatory or non-peristaltic movements. Reduction of friction by alternating expansion and contraction during peristalsis suggests higher efficiency than undulatory burrowing in compacted sediments. The limited distance over which forces can be applied during peristalsis, however, may be insufficient to overcome fracture resistance or even to anchor small worms in less consolidated sediments. Mechanics indicate that undulatory burrowing is more effective in these weak surface sediments and that these differences are greater for small worms—sediments that are too tough for small peristaltic burrowers to crack [3] exert smaller normal forces and less frictional resistance on small undulatory burrowers. These different mechanisms of burrowing in muds—plastic deformation or elastic–plastic fracture for undulatory burrowers versus elastic fracture for peristaltic burrowers (figure 6)—suggest habitat partitioning and different functional roles of infauna based on sediment mechanics and body size.

This project was funded by NSF OCE grant no. 1029160. We thank C. Hermans, P. Jumars, M. Koehl and M. Pruett for helpful discussions; T. Tucker and A. Francoeur for helping with data analysis; and S. Woodin and an anonymous reviewer for constructive feed-back on the manuscript.

References

1. Dorgan KM, Jumars PA, Johnson BD, Boudreau B, Landis E. 2005 Burrow extension by crack propagation. *Nature* **433**, 425. (doi:10.1038/nature03232)
2. Dorgan KM, Arwade S, Jumars PA. 2007 Burrowing in marine muds by crack propagation: kinematics and forces. *J. Exp. Biol.* **210**, 4198–4212. (doi:10.1242/jeb.010371)
3. Che J, Dorgan KM. 2010 It's tough to be small: dependence of burrowing kinematics on body size. *J. Exp. Biol.* **213**, 1241–1250. (doi:10.1242/jeb.038661)
4. Volkenborn N, Polerecky L, Wethey D. 2010 Oscillatory porewater bioadvection in marine sediments induced by hydraulic activities of *Arenicola marina*. *Limnol. Oceanogr.* **55**, 1231–1247. (doi:10.4319/lo.2010.55.3.1231)
5. Gray J, Lissmann HW. 1964 The locomotion of nematodes. *J. Exp. Biol.* **41**, 135–154.
6. Maladen RD, Ding Y, Li C, Goldman DI. 2009 Undulatory swimming in sand: subsurface locomotion of the sandfish lizard. *Science* **325**, 314–318. (doi:10.1126/science.1172490)
7. Gidmark NJ, Strother J, Horton J, Summers AP, Brainerd EL. 2011 Locomotory transition from water to sand and its effects on undulatory kinematics in sand lances (Ammodytidae). *J. Exp. Biol.* **214**, 657–664. (doi:10.1242/jeb.047068)
8. Herrel A, Choi H, Dumont E, de Schepper N, Vanhooydonck B, Aerts P, Adriaens D. 2011 Burrowing and subsurface locomotion in anguilliform fish: behavioral specializations and mechanical constraints. *J. Exp. Biol.* **214**, 1379–1385. (doi:10.1242/jeb.051185)
9. Dorgan KM, Jumars PA, Johnson BD, Boudreau BP. 2006 Macrofaunal burrowing: the medium is the message. *Oceanogr. Mar. Biol.* **44**, 85–121.
10. Taylor G. 1952 Analysis of the swimming of long and narrow animals. *Proc. R. Soc. Lond. A* **214**, 158–183. (doi:10.1098/rspa.1952.0159)
11. D'Aout K, Aerts P. 1999 A kinematic comparison of forward and backward swimming in the eel *Anguilla anguilla*. *J. Exp. Biol.* **202**, 1511–1521.
12. Gillis GB. 1998 Environmental effects on undulatory locomotion in the American eel *Anguilla rostrata*: kinematics in water and on land. *J. Exp. Biol.* **201**, 949–961.
13. Gray J, Hancock G. 1955 The propulsion of sea-urchin spermatozoa. *J. Exp. Biol.* **32**, 802–814.
14. Jordan CE. 1998 Scale effects in the kinematics and dynamics of swimming leeches. *Can. J. Zool.* **76**, 1869–1877. (doi:10.1139/z98-131)
15. Paul C, Halanych KM, Tiedemann R, Bleidorn C. 2010 Molecules reject an opheliid affinity for *Travisia* (Annelida). *Syst. Biodivers.* **8**, 507–512. (doi:10.1080/14772000.2010.517810)
16. Hermans CO. 1978 Metamorphosis in the opheliid polychaete *Armandia brevis*. In *Settlement and metamorphosis of marine invertebrate larvae* (eds F-S Chia, ME Rice), pp. 113–126. Amsterdam, The Netherlands: Elsevier.
17. Berri S, Boyle JH, Tassieri M, Hope IA, Cohen N. 2009 Forward locomotion of the nematode *C. elegans* is achieved through modulation of a single gait. *HFSP J.* **3**, 186–193. (doi:10.2976/1.3082260)
18. Fang-Yen C, Wyart M, Xie J, Kawai R, Kodger T, Chen S, Wen Q, Samuel A. 2010 Biomechanical analysis of gait adaptation in the nematode *Caenorhabditis elegans*. *Proc. Natl Acad. Sci. USA* **107**, 20 323–20 328. (doi:10.1073/pnas.1003016107)
19. Guo ZV, Mahadevan L. 2008 Limbless undulatory propulsion on land. *Proc. Natl. Acad. Sci. USA* **105**, 3179–3184. (doi:10.1073/pnas.0705442105)
20. Langbein W, Leopold LB. 1966 *River meanders-theory of minimum variance*. Washington, DC: United States Government Printing Office.
21. Hirose S. 1993 *Biologically inspired robots*. New York, NY: Oxford University Press.
22. Dorgan KM, Lefebvre S, Stillman J, Koehl MAR. 2011 Energetics of burrowing by the cirratulid polychaete *Cirriformia moorei*. *J. Exp. Biol.* **214**, 2202–2214. (doi:10.1242/jeb.054700)
23. Dorgan KM, Arwade S, Jumars PA. 2008 Worms as wedges: effects of sediment mechanics on burrowing behavior. *J. Mar. Res.* **66**, 219–254. (doi:10.1357/002224008785837130)
24. Johnson BD, Barry MA, Boudreau BP, Jumars PA, Dorgan KM. 2011 *In situ* tensile fracture toughness of surficial cohesive marine sediments. *Geo Mar. Lett.* **32**, 39–48. (doi:10.1007/s00367-011-0243-1)
25. Barry MA, Johnson BD, Boudreau BP. 2012 A new instrument for high-resolution *in situ* assessment of Young's modulus in shallow cohesive sediments. *Geo Mar. Lett.* **32**, 349–357. (doi:10.1007/s00367-012-0277-z)
26. Clark RB, Hermans CO. 1976 Kinetics of swimming in some smooth-bodied polychaetes. *J. Zool.* **178**, 147–159. (doi:10.1111/j.1469-7998.1976.tb06004.x)
27. Katz SL, Shadwick RE. 1998 Curvature of swimming fish midlines as an index of muscle strain suggests swimming muscle produces net positive work. *J. Theor. Biol.* **193**, 243–256. (doi:10.1006/jtbi.1998.0696)
28. McMillen T, Holmes P. 2006 An elastic rod model for anguilliform swimming. *J. Math. Biol.* **53**, 843–886. (doi:10.1007/s00285-006-0036-8)
29. Ayers J. 1989 Recovery of oscillator function following spinal regeneration in the sea lamprey. In *Cellular and neuronal oscillators* (ed. JW Jacklet), pp. 371–405. New York, NY: Marcel Dekker.
30. Jayne BC. 1988 Muscular mechanisms of snake locomotion: an electromyographic study of lateral undulation of the florida banded water snake (*Nerodia fasciata*) and the yellow rat snake (*Elaphe obsoleta*). *J. Morphol.* **197**, 159–181. (doi:10.1002/jmor.1051970204)
31. Webb J. 1973 The role of the notochord in forward and reverse swimming and burrowing in the amphioxus *Branchiostoma lanceolatum*. *J. Zool. Lond.* **170**, 325–338. (doi:10.1111/j.1469-7998.1973.tb01381.x)
32. Silvester NR, Holwill MEJ. 1972 An analysis of hypothetical flagellar waveforms. *J. Theor. Biol.* **35**, 505–523. (doi:10.1016/0022-5193(72)90148-8)